



Computational study of biomass fast pyrolysis in a fluidized bed reactor

Estudio computacional de la pirólisis rápida de biomasa en un reactor de lecho fluidizado

C.D. Ahumada¹, J.F. Hinojosa- Palafox^{1*}, V.M. Maytorena¹, C. Pérez-Rábago²

¹Universidad de Sonora, Blvd. Rosales y Luis Encinas S/N, 83000, Hermosillo, Sonora, México.

²Instituto de Energías Renovables, Universidad Nacional Autónoma de México, Privada Xochicalco S/N, 62580, Temixco, Morelos, México.

Received: February 22, 2022; Accepted: June 30, 2022

Abstract

Biofuels are considered a promising source of renewable energy. Pyrolysis uses heat in an inert atmosphere to break down biomass and produce biofuels like bio-oil (tar) and synthesis gas. This paper presents a computational study of fast biomass pyrolysis in a laboratory fluidized reactor. A laminar flow regime and an Eulerian-Eulerian approach were considered. A comprehensive kinetic model consisting of sixteen irreversible, first-order reactions was coupled with conservation equations of mass, momentum, and energy. The computational model was validated with data reported in the literature. The effect of biomass type and reactor temperature on the thermal decomposition of biomass were analyzed, finding a direct relationship between the content of cellulose and production of tar and similarly between the content of lignin and production of char. Also, the absence of lignin in the biomass dramatically changes the tar and gas compositions. Energy requirements, temperature contours, the composition of the exit gases, and final product yields (tar, char, and gas) are reported.

Keywords: computational study, fast pyrolysis, biomass, fluidized bed reactor.

Resumen

Los biocombustibles se consideran una fuente prometedora de energía renovable. La pirólisis utiliza calor en una atmósfera inerte para descomponer la biomasa y producir biocombustibles como el biopetróleo (tar) y el gas de síntesis. Este artículo presenta un estudio computacional de pirólisis rápida de biomasa en un reactor fluidizado de laboratorio. Se consideró un régimen de flujo laminar y un enfoque Euleriano-Euleriano. Un modelo exhaustivo y completo, que consta de dieciséis reacciones irreversibles de primer orden, se acopló con las ecuaciones de conservación de masa, momentum y energía. El modelo computacional fue validado con datos reportados en la literatura. Se analizó el efecto del tipo de biomasa y la temperatura del reactor sobre la descomposición térmica de la biomasa, encontrando una relación directa entre el contenido de celulosa y la producción de tar, similarmente también entre el contenido de lignina y la producción de char. Además, la ausencia de lignina en la materia prima modifica dramáticamente la composición de tar y gas obtenidos. Se reportan los requerimientos de energía, los contornos de temperatura, la composición de los gases de salida y la proporción de productos finales (alquitrán, biochar y gas).

Palabras clave: estudio computacional, pirólisis rápida, biomasa, reactor, lecho fluidizado.

* Corresponding author. E-mail: fernando.hinojosa@unison.mx

<https://doi.org/10.24275/rmiq/Cat2744>

ISSN:1665-2738, issn-e: 2395-8472

1 Introduction

Fossil fuels have various disadvantages in addition to pollution. Their principal reserves are in only a few regions globally, and their continuous supply depends on political, economic, or ecological factors (Bilgen, 2014). For this reason, it is essential to diversify fuels and energy sources, resorting to abundant renewable sources such as biofuels, solar, wind, or geothermal energy (Bhutto *et al.*, 2011). Biofuels are considered a promising source of renewable energy. A common way to obtain them is through biomass thermochemical conversion processes, such as pyrolysis, gasification, torrefaction, combustion, and distillation (Weldekidan *et al.*, 2018). Pyrolysis uses heat in an inert atmosphere to break down biomass and produce biofuels such as bio-oil or tar (pyrolysis oil) and hydrogen-rich synthesis gas. The flexibility of this process makes it possible to favor the production of bio-oil as a fuel for heat and power generation or to favor the production of synthesis gas, which can be converted into hydrogen (Morales-Diaz *et al.*, 2015, Hertwich and Zhang, 2009, Palmay-Paredes *et al.*, 2021) as well as biochar. Biochar is a porous solid that can be used for soil remediation due to its ability to adsorb organic and inorganic contaminants (Hertwich and Zhang, 2009; Xie *et al.*, 2015), heavy metals (Uchimiya *et al.*, 2011), and pesticides (Cabrera *et al.*, 2014).

Biomass pyrolysis can be divided into slow (conventional), fast, and flash, depending on residence time and heat flux. It generally follows a three-step mechanism: dehydration, primary, and secondary reactions (Kan *et al.*, 2016). Fast pyrolysis is an advanced technology gaining attention due to the growing interest in producing liquid fuels from biomass. It is a continuous process whose purpose is to prevent the gasification of most of the raw material. Fast pyrolysis mainly requires high heat transfer rates and temperatures between 450 and 600°C for residence times of a few seconds (Bridgwater, 1994; Hornung and Dasappa, 2014). Since the reactions occur quickly, the reaction kinetics and transport phenomena, alongside mass and heat transfer rate, play a crucial role in determining the obtained products. Therefore, it is necessary to set the parameters optimally to favor the formation of a particular product (Hornung and Dasappa, 2014).

On the other hand, fluidized bed reactors are used for numerous chemical processes, in which

parameters such as mass diffusion or heat transfer are fundamental. Compared to packed bed reactors, fluidized beds exhibit notable advantages such as better temperature control, greater uniformity, or longer shelf life of the solid material. A fluidized bed can achieve excellent mixing between the suspended particles and the surrounding fluid. This kind of reactor makes it possible to achieve high conversion percentages when a good mixing and heat transfer between the solid and fluid phases is required (Suleiman *et al.*, 2013).

Numerical modeling of biomass pyrolysis can be classified into two categories: microscopic scale and reactor level scale. Understanding pyrolysis at a microscopic level is essential to describe the process inside the reactor. Single-particle models are transport equations that couple reaction kinetics with mathematical descriptions of mass and heat transfer during thermochemical conversion (Yang *et al.*, 2008). Most of these types of microscopic studies focus on characterizing heat and mass transfer within a single biomass particle (Janse *et al.*, 2000). Numerous studies analyze the effect of the shape and size of biomass particles since they are considered determining factors in pyrolysis reactions (Yang *et al.*, 2008). Gera *et al.* (2002) proposed a combustion model for a biomass particle with significantly large aspect ratios to investigate the temperature distribution within the particle. These studies have provided relevant information about biomass pyrolysis and contributed to a better understanding of the thermochemical conversion in individual particles due to their relative simplicity and ease of validation through experimental comparisons. However, single-particle models are not sufficient to be applied in the description of pyrolysis in a complete reactor, where interactions between solid and gas phases are crucial.

The thermodynamic equilibrium approach has been used in several studies, such as Baggio *et al.* (2009), which minimizes the problem by finding a final composition that results in the total minimum Gibbs free energy. Baratieri *et al.* (2008) used a two-phase thermodynamic equilibrium model to predict pyrolysis and biomass gasification. However, the main limitation of this approach is the assumption of the equilibrium condition, which is reached in a very long time, in addition to the fact that the equilibrium models are unable to provide information about the flow and concentration distributions of the species inside the reactor (Aramideh *et al.*, 2015).

Computational fluid dynamics (CFD) has proven to be an efficient tool for simulating the complex

phenomena during biomass pyrolysis. Wagenaar *et al.* (1994) studied the fast pyrolysis of biomass in a rotating cone reactor by integrating a flow model with reaction kinetics for the pyrolysis of wood. Various computational studies have described pyrolysis processes in fluidized bed reactors using CFD, such as Di Blasi (2000) and Anca-Couce *et al.* (2013). Studies with a CFD approach can be of the Lagrangian-Eulerian or Eulerian-Eulerian type. Papadikis *et al.* (2009) studied the fast pyrolysis of biomass in a drag flow reactor in which the presence of sand was neglected, and biomass particles were considered with a Lagrangian approach, while the gas phase is described with the Eulerian approach. Instead, other studies have used the Eulerian-Eulerian method to efficiently simulate many solid particles in fluidized bed reactors. Xue *et al.* (2011) proposed an Eulerian-Eulerian approach to simulate the fast pyrolysis of biomass in a bubbling fluidized-bed reactor in conjunction with granular flow kinetic theory to calculate solid-phase properties coupled with reaction kinetics. Recently Xiong *et al.* (2013) and Aramideh *et al.* (2015) have developed CFD modeling in OpenFOAM to study biomass fast pyrolysis in fluidized-bed and screw-type reactors, coupling reaction kinetics with multiphase transport models. Other works such as Ranganathan and Gu (2016) and Mellin *et al.* (2014) have used commercial CFD codes (ANSYS Fluent) with Eulerian-Eulerian approaches in conjunction with relatively complex kinetic models to describe pyrolysis processes in fluidized bed reactors successfully.

The literature review shows that several studies on computational modeling of biomass pyrolysis have been reported. However, no investigation of the fast pyrolysis of biomass in a fluidized bed reactor was found using a detailed kinetic model and focusing on the effect of biomass types and reactor temperature. Therefore, the objective of the present study is to develop a validated computational model to analyze biomass type and reactor temperature's effect on the thermal decomposition of biomass in a laboratory-scale fluidized-bed reactor. The manuscript was organized into the following sections: (1) Introduction, (2) Definition of the physical system, (3) Assumptions and mathematical model, (4) Kinetic model, (5) Numerical methodology, (6) Results and discussion and (7) Conclusions. An Eulerian-Eulerian approach was considered. The kinetic model of Ranzi *et al.* (2008) was coupled with equations based on conservation principles of mass, momentum, and energy. The computational model was validated with

data reported in the literature. Energy requirements, the composition of the exit gases, temperature contours, and product yields (tar, char, and gas) are reported.

2 Definition of the physical problem

A real system for pyrolysis operations in a fluidized bed reactor consists of various equipment such as preheaters, condensers, or cyclone separators. In this work, the system is limited to the reactor, where the pyrolysis reactions are carried out, as shown in Figure 1. The reactor geometry and construction material are based on a 300 g/h fluidized bed reactor used by Kalgo (2011), whose study has reported experimental data considered in this paper for validation purposes. The reactor has a nitrogen inlet at the bottom and a biomass inlet at the bottom of the left sidewall. Non-slip was considered in the walls for the gas phase and a specular coefficient of 0.5 for sand and biomass. A constant temperature was taken on the walls of the reactor. The construction material of the walls was established as nickel, which corresponds to the reactor's material studied by Kalgo (2011). Nitrogen input was considered at a constant velocity and temperature. It was assumed that the gases leave at atmospheric pressure and that the biomass enters with a continuous and constant mass flow.

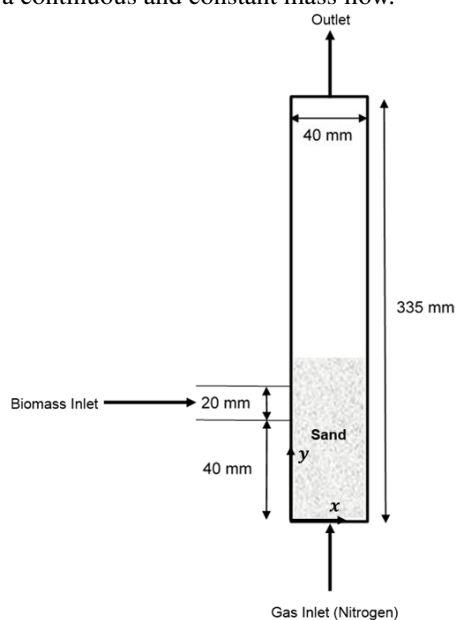


Figure 1. Scheme of the physical problem.

3 Assumptions and mathematical model

The mathematical modeling of biomass fast pyrolysis in a fluid bed reactor is complex. Therefore, to obtain the governing equations, we made the following assumptions:

- The problem may be described as two-dimensional.
- Gas-phase is treated as an ideal gas.
- The flow regimen is laminar ($Re < 200$).
- The reactor behaves as a dispersed heterogeneous system.
- The solid and gas phases are continuous.
- The flow in solid phases is granular.

The fluid and solid motions coupled with heat and mass transfer inside the reactor were described with a microscopic application of mass conservation (global and for each chemical specie), the second law of Newton, and the first law of Thermodynamics. The governing equations for the gas and solid phases are presented below in Table 1, along with constitutive relationships (Table 2) using a Eulerian-Eulerian approach (Papadakis et al. (2009)).

The subscript g in equation of continuity (Eq. 1) denotes the gas phase, and α , ρ , and U represent a volumetric fraction, density, and velocity. Furthermore, R_{gsm} is the source term that considers

heterogeneous reactions between the gas and solid phases. β_{gsm} in equation of momentum (Eq. 2) represents the momentum transfer coefficient between the gas phase and the solid phase, similarly ψ_{gsm} refers to the exchange of momentum due to chemical reactions between phases. The stress tensor τ_g is defined in equation (9), where μ_g , λ_g , \mathbf{I} , and D_g are the dynamic viscosity, the volumetric viscosity, the identity tensor, and the stress tensor of the gas phase, respectively. The drag forces β_{gsm} can be calculated by different models proposed through empirical correlations, the two main ones being Gidaspow (1994) and Syamlal et al. (1993). Momentum transport by chemical reactions is defined in equation (10).

In equation of energy conservation (Eq. 3), the heat flux by conduction (\mathbf{q}_g) is computed with equation (11). The heat transfer between the phases due to chemical reactions (X_{gsm}) is evaluated with equations (12) and (13).

In equation of mass conservation for each specie (Eq. 4) Y_{gk} is the mass fraction of the K species. R_{gk} corresponds to the generation of matter of the K species considering all the heterogeneous reactions between phases. The diffusive flux is calculated using Fick's law.

For solid phases, in equation of continuity (Eq 5), R_{sm} represents the generation of matter due to all chemical reactions between the solid phase m and other phases. Momentum transport is defined by equation 6 where β_{gsm} is the momentum transfer coefficient between the gas phase and the solid phase m and β_{slm} is the momentum transfer coefficient between the solid phase m and another solid phase l. The stress tensor, τ_{sm} , is defined by equation (15).

Table 1. Governing equations.

Gas	Continuity	$\frac{\partial \alpha_g \rho_g}{\partial t} + \nabla \cdot (\alpha_g \rho_g \mathbf{U}_g) = \sum_{m=1}^M R_{gsm}$	(1)
Phase	Momentum	$\frac{\partial \alpha_g \rho_g \mathbf{U}_g}{\partial t} + \nabla \cdot (\alpha_g \rho_g \mathbf{U}_g \mathbf{U}_g) = \nabla \cdot \tau_g - \alpha_g \nabla p_g + \sum_{m=1}^M \beta_{gsm} (\mathbf{U}_{sm} - \mathbf{U}_g) + \sum_{m=1}^M \psi_{gsm} + \alpha_g \rho_g \mathbf{g}$	(2)
	Energy	$\frac{\partial \alpha_g \rho_g C_{pg} T_g}{\partial t} + \nabla \cdot (\alpha_g \rho_g C_{pg} T_g \mathbf{U}_g) = \nabla \cdot \mathbf{q}_g + \sum_{m=1}^M h_{gsm} (T_{sm} - T_g) + \sum_{m=1}^M X_{gsm} + \Delta H_g$	(3)
	Species	$\frac{\partial \alpha_g \rho_g Y_{gk}}{\partial t} + \nabla \cdot (\alpha_g \rho_g Y_{gk} \mathbf{U}_g) = \nabla \cdot \mathbf{j}_{gk} + R_{gk}$	(4)
Solid	Continuity	$\frac{\partial \alpha_{sm} \rho_{sm}}{\partial t} + \nabla \cdot (\alpha_{sm} \rho_{sm} \mathbf{U}_{sm}) = R_{sm}$	(5)
Phase	Momentum	$\frac{\partial \alpha_{sm} \rho_{sm} \mathbf{U}_{sm}}{\partial t} + \nabla \cdot (\alpha_{sm} \rho_{sm} \mathbf{U}_{sm} \mathbf{U}_{sm}) = \nabla \cdot \tau_{sm} - \alpha_{sm} \nabla p_{sm} + \beta_{gsm} (\mathbf{U}_g - \mathbf{U}_{sm}) + \sum_{l=1, l \neq m}^M \beta_{slm} (\mathbf{U}_{sl} - \mathbf{U}_{sm}) + \psi_{sm} + \alpha_{sm} \rho_{sm} \mathbf{g}$	(6)
	Energy	$\frac{\partial \alpha_{sm} \rho_{sm} C_{psm} T_{sm}}{\partial t} + \nabla \cdot (\alpha_{sm} \rho_{sm} C_{psm} T_{sm} \mathbf{U}_{sm}) = \nabla \cdot \mathbf{q}_{sm} + h_{gsm} (T_g - T_{sm}) + X_{sm} + \Delta H_{sm}$	(7)
	Species	$\frac{\partial \alpha_{sm} \rho_{sm} Y_{smk}}{\partial t} + \nabla \cdot (\alpha_{sm} \rho_{sm} Y_{smk} \mathbf{U}_{sm}) = R_{smk}$	(8)

Table 2. Constitutive equations.

Gas phase	Stress tensor	$\tau_g = 2\alpha_g\mu_g D_g + \alpha_g\lambda_g tr(D_g)\mathbf{I}$	(9)
	Momentum transport	$\psi_{gsm} = R_{gsm}[\xi U_{sm} + (1 - \xi)U_g]$	
	by chemical reactions	$\xi = \begin{cases} 0, & R_{gsm} < 0 \\ 1, & R_{gsm} \geq 0 \end{cases}$	(10)
	Heat flux by conduction	$\mathbf{q}_g = \alpha_g\kappa_g \nabla T_g$	(11)
	Heat transport by	$X_{gsm} = R_{gsm}[\xi C_{p sm} T_{sm} + (1 - \xi)C_{pg} T_g]$	(12)
	chemical reactions	$\xi = \begin{cases} 0, & R_{gsm} < 0 \\ 1, & R_{gsm} \geq 0 \end{cases}$	(13)
	Diffusive flux	$\mathbf{j}_{gk} = \alpha_g \rho_g D_{gk} \nabla Y_{gk}$	(14)
Solid phase	Stress tensor	$\tau_{sm} = -p_{sm}\mathbf{I} + 2\alpha_{sm}\mu_{sm}D_{sm} + \alpha_{sm}\lambda_{sm}tr(D_{sm})\mathbf{I}$	(15)
	Pressure of solids	$p_{sm} = 2\alpha_{sm}^2 \rho_{sm} \theta_{sm} g_{0sm} (1 + e)$	(16)
	Volumetric viscosity	$\lambda_{sm} = \frac{4}{3} \alpha_{sm}^2 \rho_{sm} g_{0sm} d_{sm} (1 + e) \sqrt{\theta_{sm}/\pi}$	(17)
	Dynamic viscosity	$\mu_{sm} = \frac{4}{5} \alpha_{sm}^2 \rho_{sm} g_{0sm} d_{sm} (1 + e) \sqrt{\frac{\theta_{sm}}{\pi} + \frac{10\rho_{sm}d_{sm}\sqrt{\theta_{sm}\pi}}{96(1+e)g_{0sm}}} \left[1 + \frac{4}{5}\alpha_{sm}(1+e)\right]^2$	(18)
	Momentum transport	$\beta_{slm} = \frac{3(1+e_{lm})\left(\frac{\pi}{2} + \frac{C_{flm}\pi^2}{8}\right)\alpha_{sm}\alpha_{sl}\rho_{sm}\rho_{sl}(d_{sl}+d_{sm})^2 g_{0slm} U_{sl}-U_{sm} }{2\pi(\rho_{sl}d_{sl}^3 + \rho_{sm}d_{sm}^3)}$	(19)
	between solid phases m and l	$g_{0slm} = \frac{1}{\alpha_g} + 3 \left[\sum_{l=1}^M \frac{\alpha_{sl}}{d_{sl}} \right] \frac{d_{sl}d_{sm}}{\alpha_g^2(d_{sl}+d_{sm})}$	(20)
	Heat flux by conduction	$\mathbf{q}_{sm} = \alpha_{sm}\kappa_{sm} \nabla T_{sm}$	(21)

Table 3. Boundary conditions for all cases.

Boundary	Boundary condition	Case 1	Case 2	Case 3	Case 4	Case 5
	N ₂ Shear	No slip				
	Solids specularity coefficient	0.5	0.5	0.5	0.5	0.5
	Sand specularity coefficient	0.5	0.5	0.5	0.5	0.5
Wall	Temperature (K)	773	773	773	873	973
	N ₂ velocity (m/s)	0.507	0.507	0.507	0.507	0.507
Inlet	N ₂ Temperature (K)	773	773	773	873	973
	Mass flow rate (kg/s)	8.33 × 10 ⁻⁵				
Biomass inlet	Biomass type	Beechwood	Cotton waste	Sugarcane bagasse	Beechwood	Beechwood
Outlet	Outlet	Pressure outlet	Pressure outlet	Pressure outlet	Pressure outlet	Pressure outlet

In this approach, the kinetic theory of granular flow (KTGF) is used to describe the tensor τ_{sm} . Granular temperature replaces the thermodynamic temperature in this case. Solid properties such as granular pressure (p_{sm}), dynamic viscosity (μ_{sm}), and volumetric viscosity (λ_{sm}) are expressed as a function of granular temperature (θ). The constitutive relationships are derived by Lun *et al.* (1984) and Gidaspow (1994).

According to Gidaspow (1994), the pressure

of solids is described in equation (16), while the volumetric viscosity of the solid phase m is equation (17). The dynamic viscosity of the solid phase m is presented in equation (18). The term β_{slm} is defined in equation (19), and it describes momentum transport between the solid phases m and l , whereas heat flux by conduction in the solid phases is described in equation (21). Boundary conditions are described in Table 3 for each of the cases studied in this paper.

Table 4. Comprehensive kinetic model for lignocellulosic biomass pyrolysis (Ranzi *et al.*, 2008).

Reaction	A (s ⁻¹)	E (kJ/mol)
1 Cellulose → Act.Cellulose	8x10 ¹³	192.5
2 Cellulose → 5H ₂ O + 6Char	8x10 ⁷	125.5
3 Act.Cellulose → LVG	4T	41.8
4 Act.Cellulose → 0.95HAA + 0.25Glyoxal + 0.2Acetaldehyde + 0.25HMFU + 0.2Acetone + 0.16CO ₂ + 0.23CO + 0.9H ₂ O + 0.1CH ₄ + 0.61Char	1x10 ⁹	133.9
5 Hemicellulose → 0.4Act.Hemicellulose 1 + 0.6Act.Hemicellulose 2	1x10 ¹⁰	129.7
6 Act.Hemicellulose 1 → 0.75H ₂ + 0.8CO ₂ + 1.4CO + 0.5Formaldehyde	3x10 ⁹	113
7 Act.Hemicellulose 1 → Xylan	3T	46
8 Act.Hemicellulose 2 → CO ₂ + 0.5CH ₄ + 0.25C ₂ H ₄ + 0.8CO + 0.8H ₂ + 0.7Formaldehyde + 0.25Methanol + 0.125Ethanol + 0.125H ₂ O + Char	1x10 ¹⁰	138.1
9 LigC → 0.35LigCC + 0.1pCoumaryl + 0.08Phenol + 0.41C ₂ H ₄ + H ₂ O + 0.495CH ₄ + 0.32CO + CO + H ₂ + 5.735Char	4x10 ¹⁵	202.9
10 LigH → LigOH + Acetone	2x10 ¹³	156.9
11 LigO → LigOH + CO ₂	1x10 ⁹	106.7
12 LigCC → 0.3pCoumaryl + 0.2Phenol + 0.35Acrylic Acid + 0.7H ₂ O + 0.65CH ₄ + 0.6C ₂ H ₄ + 1.8CO + H ₂ + 6.4Char	5x10 ⁶	131.8
13 LigOH → Lign + H ₂ O + Methanol + 0.45CH ₄ + 0.2C ₂ H ₄ + 2CO + 0.7H ₂ + 4.15Char	3x10 ⁸	125.5
14 Lign → LumpedPhenol	8T	50.2
15 Lign → H ₂ O + 2CO + 0.2Formaldehyde + 0.4Methanol + 0.2Acetaldehyde + 0.2Acetone + 0.6CH ₄ + 0.65C ₂ H ₄ + 0.5H ₂ + 5.5Char	1.2x10 ⁹	125.5
16 H ₂ O _(l) → H ₂ O _(g)	5.3x10 ¹⁰	88

4 Kinetic model

In this work, the kinetic model of Ranzi *et al.* (2008) was selected since it offers a more rigorous and detailed description than global and simple generalized models (Table 4). Only primary chemical reactions are considered in this study, as it has been shown by Trendewicz *et al.* (2014) that for fast pyrolysis operations, the contribution of secondary chemical reactions is not significant in the description of kinetics. This model makes some relevant considerations. One of the main ones is that, due to the complexity and diversity of lignin, it is classified into three types (LigC, LigO, and LigH) according to its composition in terms of Carbon, Hydrogen, and Oxygen. Furthermore, the Arrhenius equation describes all sixteen reactions of the kinetic model are irreversible, first order, and reaction rate constants.

5 Numerical methodology

Considering that the description of the physical problem involves a complex system of partial differential equations, which do not have an analytical solution, it is necessary to resort to numerical methods that involve solving the equations using computers. ANSYS Fluent v18 computational fluid dynamics software was used in this study. The SIMPLE algorithm was used to couple the continuity and momentum equations. Advective terms were discretized with a second-order upwind scheme. Temporal discretization was performed with an implicit first-order scheme. A mesh independence study was carried out to determine the optimal mesh. Four structured and uniform meshes were generated under the following characteristics: 45x342, 48x361, 50x380, 53x399 (width x height elements). The reactor wall was maintained at a temperature of 973 K and fed with a nitrogen current of 0.507 m/s at the same operating temperature of the reactor. The simulations were performed with a time step of 0.00001 s. The y-component profiles of the velocity (mean-y-velocity) in the gas phase were compared (Figure 2a). The profiles were generated at the height of 251.25 mm at 3 s of operation. As can be seen, the implemented meshes show little variation. The relative mean differences between the profiles were less than 0.12%. The profiles corresponding to the average

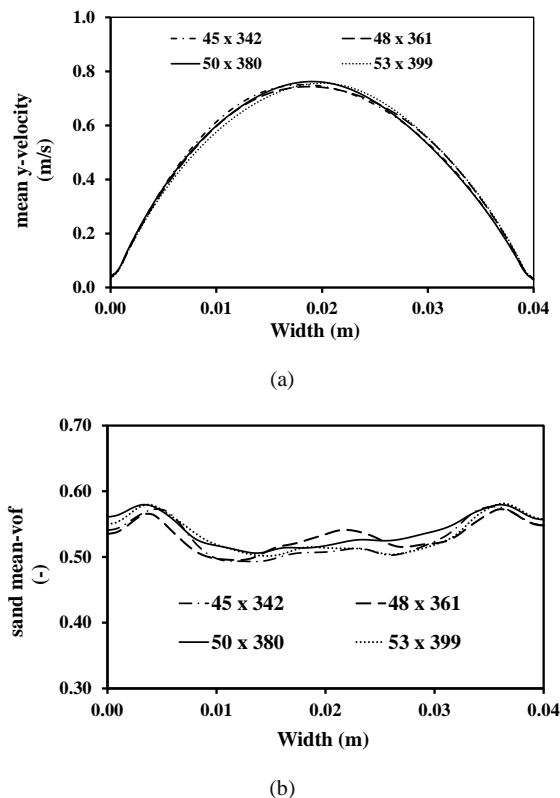


Figure 2. Comparison between the profiles generated by the different meshes: (a) mean-y-velocity and (b) sand mean volume fraction (mean-vof), at a time of 3 s.

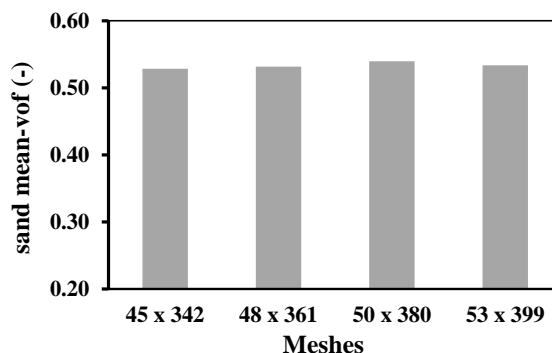


Figure 3 Comparison between the average values of the sand mean volume fraction at a time of 3 s.

volumetric fraction of the sand (sand-mean-vof) were also compared. These profiles were generated at the height of 50 mm at 3 s of operation (Figure 2b). The relative mean differences between these profiles were no more than 1.6%. The relative mean difference between the 53x399 and 50x380 mesh is 1.1% (Figure 3). Based on the previous results, it is concluded that

using a mesh of 50x380 elements is representative and independent of the phenomenon studied. Six seconds were simulated with a time step of 0.00001 s to assure computational stability. To carry out the complete study involving pyrolysis reactions, it was necessary to establish the existence of 3 Eulerian phases: two solid and one gaseous, among which are all the species involved, whether they are reactants, products, intermediate or inert species.

Drag forces are described by Syamlal *et al.* (1993) correlation. Heat transfer between the gas phase and sand is explained by the correlation of Gunn (1978), while heat transfer between gas and solid phase (biomass) is computed with the correlation of Ranz and Marshall (1952). The coefficient of restitution to describe collisions between all solid phases is 0.9. Since transport properties apply to the entire gas phase, it is only necessary to specify standard molecular weights and enthalpies of formation for individual species. Similarly, in the solid phase are several species, of which it is required to determine molecular weight and standard enthalpy of formation. Due to the complexity of this detailed kinetic model, which is characterized by the addition of three types of lignin and active species of cellulose and hemicellulose, and considering the limited availability of these specific data, properties predicted by Gorenssek *et al.* (2019) are chosen for the solid phase. Required properties are shown in Tables 5 and 6.

To obtain the main results, which are the product yields (char, tar, and gas), the total mass of solid and gas phases was obtained by carrying out volume integrals:

$$\int \alpha_p \rho_p dV = \sum_{i=1}^n \alpha_{p_i} \rho_{p_i} |V_i| \quad (22)$$

Where p is the corresponding phase, i is the cell where the calculation is performed, and V is the volume of each cell in the domain. Subsequently, the mass fraction of each species that is classified as a product is obtained through a volume-averaged average:

$$\frac{1}{V} \int \varphi dV = \frac{1}{V} \sum_{i=1}^n \varphi_i |V_i| \quad (23)$$

Where φ is the variable of interest, the mass fraction of each species. Finally, the mass fraction of the species is multiplied by the total mass of the phase in which they are found to calculate the mass of each species individually. Once the masses of all the species are obtained, they are added to get the total mass of products. They are also grouped into char, tar, or gas.

In this way, the total fractions of products can be obtained as suggested by the following equations:

$$X_{Char} = \frac{m_{Char}}{m_{Char} + m_{Gas} + m_{Tar}} \quad (24)$$

$$X_{Gas} = \frac{m_{Gas}}{m_{Char} + m_{Gas} + m_{Tar}} \quad (25)$$

$$X_{Tar} = \frac{m_{Tar}}{m_{Char} + m_{Gas} + m_{Tar}} \quad (26)$$

Where X represents the fraction of each product and m the mass of the products.

Regarding the types of biomasses, beechwood was selected as Case 1 due to the data availability compared with other studies reported in the literature. The second type of biomass consists of the typical cotton gin residues, composed almost entirely of cellulose, and does not contain lignin (Table 7). Sugar cane bagasse was chosen as the third type. However, it maintains similar percentages to Case 1. It has less lignin and increases inert materials compared to the other two biomass classes.

Table 5. Properties of the gas phase.

Density (kg/m ³)	Ideal Gas
Specific heat capacity (J/kgK)	$C_p = 979.043 + 0.4179639T - 0.001176279T^2 + 1.674394 \times 10^{-6}T^3 - 7.256297 \times 10^{-10}T^{-4}$
Viscosity (kg/ms)	$\mu = \mu_0(T/T_0)^{3/2}(T_0 + C)/(T + C)$ $\mu_0 = 1.7984 \times 10^{-5}, T_0 = 273.11K, C = 110.56$
Thermal conductivity (W/mK)	0.0454

Table 6. Properties of sand and solids.

Property	Sand	Solids
Density (kg/m ³)	2670	680
Char density (kg/m ³)	—	300
Specific heat capacity (J/kg K)	830	1500
Thermal conductivity (W/m K)	0.25	0.105
Particle size (m)	0.000725	0.000625
Granular viscosity (kg/m s)	Syamlal <i>et al.</i> (1993)	Syamlal <i>et al.</i> (1993)
Volumetric granular viscosity (kg/m s)	Lun <i>et al.</i> (1984)	Lun <i>et al.</i> (1984)
Frictional viscosity (kg/m.s)	Schaeffer (1987)	Schaeffer (1987)
Frictional pressure (Pa)	Syamlal <i>et al.</i> (1993)	Syamlal <i>et al.</i> (1993)
Granular temperature (m ² /s ²)	Algebraic	Algebraic
Solids pressure (Pa)	Syamlal <i>et al.</i> (1993)	Syamlal <i>et al.</i> (1993)
Radial distribution	Syamlal <i>et al.</i> (1993)	Syamlal <i>et al.</i> (1993)
Modulus of elasticity (Pa)	Derived	Derived
Packing limit	0.6	0.4

Table 7. Composition of the three types of biomasses to study.

Biomass	Cellulose (%)	Hemicellulose (%)	LigC (%)	LigO (%)	LigH (%)	Humidity (%)	Inert (%)	Source
Case 1: Beechwood	40.1	26.8	11	0	12	9.4	0.7	(Rossi, 1984)
Case 2: Cotton waste	73.60	15.14	-	-	-	5.86	5.4	(Raveendran <i>et al.</i> , 1995)
Case 3: Sugarcane bagasse	41.5	24.5	8.11	0	9.39	9.95	6.55	(Kalgo, 2011)

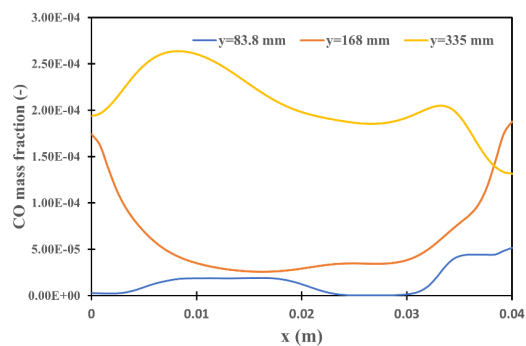
6 Results and discussion

6.1 Validation of the computational model

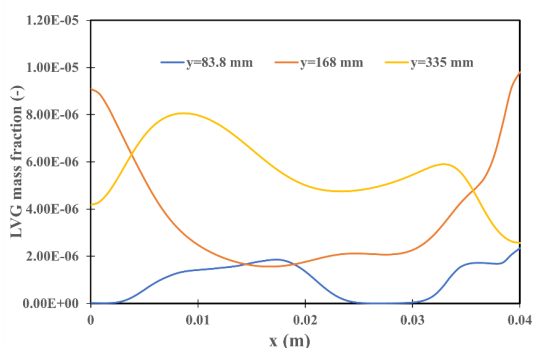
Pyrolysis of beech wood (Case 1) has been compared to both the results of product yields reported by Ranganathan and Gu (2016) and the experimental data of Kalgo (2011). The production of all the species derived from the chemical reactions defined in the kinetic model is observed. Such is the case of CO, char, or levoglucosan, as exemplified in Figure 4. Gaseous species are flowing to the outlet, and char is fluidizing between the sand bed. Also, gaseous species follow a similar behaviour with low concentration values at $y=83.8$ mm, which is closer to the biomass feed, that means biomass is starting to increase its temperature and react but not with a high production of gaseous products yet. At $y=168$ mm, which is the middle part of the reactor, there are slightly higher concentration values in general and some very high values near the walls, which are the zones with the highest temperature of the reactor. In a height of 335 mm, the maximum concentration values are found because the biomass that is inside the reactor was heated enough to react and all gaseous products were carried to the outlet, as shown in Figures 4a and

b. It observed in Figure 4c that while biomass is being fed ($y=50$ mm) there is no production of char until it gets closer to the opposite wall of the reactor, that is when it reaches a higher temperature, enough to start pyrolysis reactions. Then at $y=83.8$ mm the highest concentration values of char can be found, because there is more heated biomass reacting; $y=111$ mm is closer to the final part of the bed and there is almost no char anymore except near the right wall where at that moment there is still biomass fluidizing and reacting to produce char.

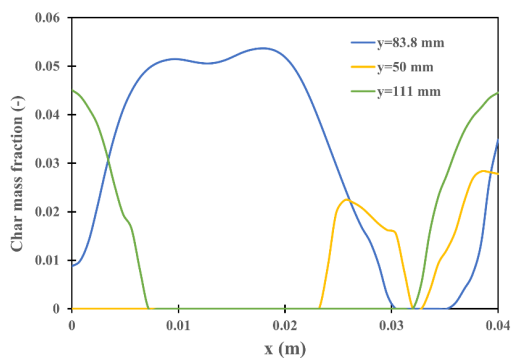
The yields of the products were calculated and compared with the experimental data of Kalgo (2011) and the numerical results reported by Ranganathan and Gu (2016). The comparison is shown in Figure 5. As can be seen, the results obtained in this work reproduce the experimental behavior in the generation of the products, predominantly the production of tar, followed by char and finally gas. When comparing these results, it was found that the best prediction is given for X_{Gas} , followed by X_{Tar} , presenting relative differences of 3.9% and 15.9%, respectively. These results are closer to the experimental data than the numerical predictions of the advanced model of Ranganathan and Gu (2016), which presented relative differences of -6.6% and 13.3%, highlighting that the present work better predicts the gas products.



(a)



(b)



(c)

Figure 4. Mass fraction profiles of representative products (a) CO, (b) Levoglucosan, and (c) char.

On the other hand, the product with the least precision was X_{Char} , with an absolute difference of 0.046, concerning the experimental data, which presents significant improvements in the prediction of Char generation with respect to the Simple (0.169) and Global (0.203), and competes with the advanced model (0.024). It makes evident that implementing a detailed kinetic model of Ranzi *et al.* (2008) together with CFD tools results in a valid approach to describe the pyrolysis of lignocellulosic biomass in a fluidized bed reactor at a laboratory scale.

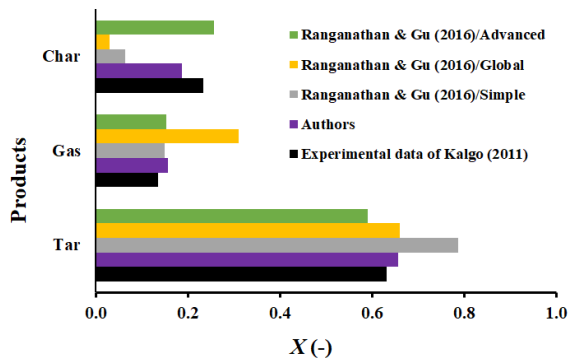


Figure 5. Comparison of products obtained in this work with literature.

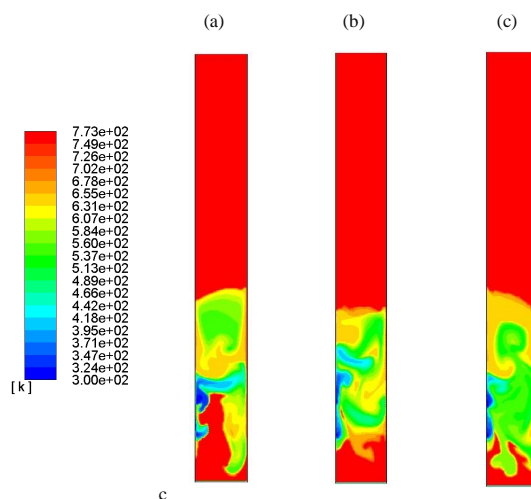


Figure 6. Solid-phase temperature contours in Case 1 (a), Case 2 (b), and Case 3 (c).

6.2 Effect of biomass composition

This section analyzes the effect of the biomass composition, emphasizing heat transfer and final product yields depending on the initial composition of biomass fed to the reactor. All results correspond to three seconds. Figure 6 shows that instantaneous temperature contours are similar for all three cases. However, in Case 2 (cotton residue), there are fewer low and medium temperature zones because the predominant cellulose is relatively easier to decompose since it is not as rigid as lignin. The latter can also be observed since the heat flux required by Case 2 to maintain a wall temperature of 773 K is slightly lower than in cases that contain a lower proportion of cellulose and higher percentages of hemicellulose and lignin. Those heat flux values are 0.216 W, 0.193 W, and 0.219 W for Cases 1, 2, and 3.

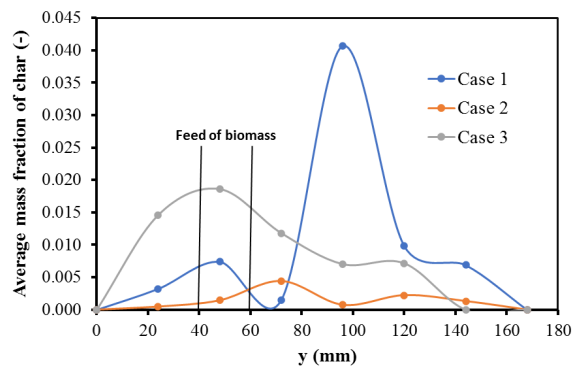


Figure 7. Variation of average mass fraction of char with the height of the reactor for Case 1, Case 2, and Case 3.

Table 8. Comparison of the percentages of final products in Cases 1, 2 and 3.

Product	Case 1	Case 2	Case 3
Tar (%)	65.63	85.85	75.18
Gas (%)	15.72	9.66	14.42
Char (%)	18.65	4.49	10.40

Figure 7 shows the variation of the average char mass fraction with the height of the reactor. Each dot represents a spatial average in the x-direction. It is observed that Case 1 presents higher mass fractions above $y=80$ mm with a maximum of 0.042%, whereas below $y=80$ mm, Case 3 reports larger mass fractions than Cases 1 and 2. In the entrance zone, Case 3 presents its highest value of about 0.018%. However, in the whole fluidized area, Case 1 has the highest char production, which its superior proportion of lignin may explain. Table 8 shows the final product yields for the three cases. A significant increase in tar for Case 2 is evident, exceeding Case 1 by 20%, and a considerable decrease in the percentage of gas is also relevant between these two, up to 6%. Also, a char reduction of 14% is observed in Case 2 compared to Case 1. It is possible to identify a direct relationship between the production of tar and cellulose content in the raw material fed to the reactor. Similarly, a lower lignin content, or its absence, means poor char production. In Case 3 (sugarcane bagasse), tar production increased by about 10%, non-condensable gas remained almost constant, and char decreased by less than 8% compared to case 1. It is reasonable since the compositions between the two cases are relatively similar. The above allows establishing a

direct relationship between the species present in biomass and the final products. In Case 3 again, sugar cane contains 5% less lignin than beech wood in case 1, and its char production decreases by 8%.

Table 9 shows the gas phase composition at the reactor outlet for all three cases. It is observed that water vapor, xylan, and acetone constitute a large part of the tar in cases 1 and 3, unlike Case 2, in which acetone has less contribution, giving way to water vapor, xylan, and formaldehyde as the main species. For non-condensable gas, it is evident that CO and CO₂ are the species with the most significant contribution in all cases.

6.3 Effect of reactor wall temperature

In this section, an analysis of the effect of reactor wall temperature is carried out. Wall temperature was modified to make a comparison between Case 1 (773 K), Case 4 (873 K), and Case 5 (973 K) to observe the effect that this parameter has concerning the general behavior of the system, emphasizing the yields of the final products. In Figure 8, instantaneous temperature profiles for the solid phase are presented at $y=83$ mm. Although the temperature limits are different, a boundary layer behavior is observed close to the lateral walls in three cases. In the core of the reactor, temperatures of the solid phase vary between 550 and 650 °C.

Figure 9 shows the instantaneous mass fraction profiles of CO, CH₄, and H₂ at the reactor outlet for Cases 1, 4, and 5. It is observed that for the three chemical species, Case 4 presents lower concentrations. However, Case 1 reports almost four times the concentrations of Case 5, except close to the right wall, where mass fractions of Case 5 surpass those of Case 1. For CH₄ and H₂, the behavior is similar, mass fractions of Case 1 are about two times those of Case 5 in the left middle section, but in the right middle section, the behavior reverses.

In this pyrolysis process, there are exothermic and endothermic reactions. However, there is a consistent behavior in which endothermic nature predominates. The instantaneous heat fluxes in the walls are 0.22 W, 0.554 W, and 28.34 W for cases 1, 4, and 5, respectively. In the three cases, a positive value denotes a heat input to compensate for the energy consumed in the reactions. Regarding results, the final product yields are presented in Table 10. Tar and Gas tend to reduce their contribution with increasing wall temperature, while char rises considerably.

Table 9. Mass fraction composition of the products in the gas phase at the reactor outlet (nitrogen was not considered) for Cases 1, 2, and 3.

Chemical species	Case 1 (%)	Case 2 (%)	Case 3 (%)
CH ₄	0.263694	0.043888	0.196022
H ₂	0.058642	0.008827	0.042946
CO	10.852298	3.921505	8.893792
C ₂ H ₄	0.291672	0.038374	0.209817
CO ₂	9.671026	3.651566	8.020601
Phenol	0.102058	0	0.064237
CH ₂ O	4.165245	1.569365	3.454345
Methanol	0.185599	0.043825	0.149620
Ethanol	0.105714	0.031508	0.087501
Acetone	6.015872	0.000171	3.505624
Acetaldehyde	0.000355	0.000129	0.000350
Lumped Phenol	0.009604	0	0.009682
Acrylic acid	0.000002	0	0.000002
P-Coumaryl alcohol	0.203557	0	0.128123
Xylan	8.587439	5.048432	8.850818
HMFU	0.000765	0.000463	0.000809
Glyoxal	0.000352	0.000213	0.000372
Levoglucosan	0.295517	0.240906	0.373039
HAA	0.001385	0.000838	0.001464
H ₂ O	59.189202	85.399989	66.010834

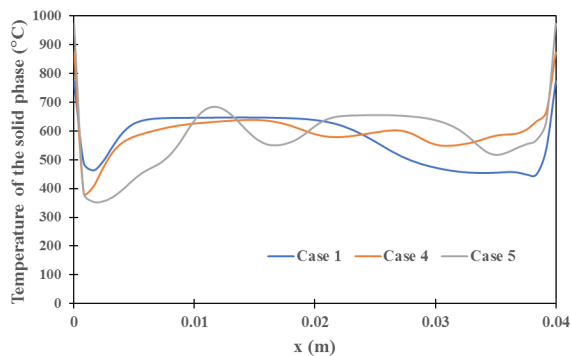


Figure 8. Temperature profiles in the solid phase at y=83 mm for Case 1, Case 4, and Case 5.

Table 10. Comparison of the percentages of final products in Cases 1, 4 and 5.

Product	Case 1 (773 K)	Case 4 (873 K)	Case 5 (973 K)
Tar (%)	65.63	59.01	45.55
Gas (%)	15.72	8.51	7.95
Char (%)	18.65	32.48	46.50

Conclusions

A detailed computational model was developed to study the fast pyrolysis of biomass in a fluidized bed reactor. Adapting the detailed kinetic model of Ranzi *et al.* (2008) in conjunction with computational fluid dynamics (CFD) has resulted in a set of reliable predictions to simulate the fast pyrolysis lignocellulosic biomass in a laboratory-scale fluidized bed reactor in reasonable agreement with experimental data. The study of biomass types allows identifying a direct relationship between tar production and cellulose content. The content of lignin in the biomass is directly related to char production in fast pyrolysis processes since cases with the highest lignin content presented a higher char output and, in turn, the case in which there was no lignin at all returned the least char output. Biomass with high cellulose content resulted in higher tar production, while biomass without lignin produced the least char among the compared cases. The absence of lignin makes an important change in tar composition, reducing acetone's contribution and letting formaldehyde become more relevant. The non-condensable gas is composed mainly of CO and CO₂ in all cases. Also, an increase in wall reactor temperatures results in a lower production of tar and

gas, but it also turns into a significant rise in char production.

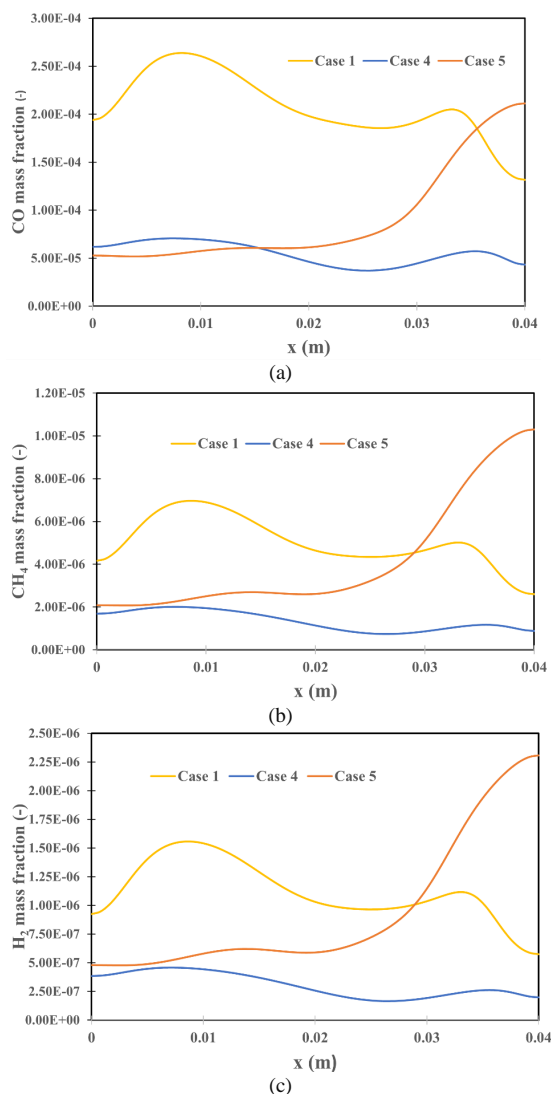


Figure 9. Comparison of mass fraction profiles of Case 1, Case 4, and Case 5 at the outlet for (a) CO, (b) CH₄, and (c) H₂.

Acknowledgments

The authors acknowledge the financial support from CONACYT-Mexico through graduate scholarships granted to C.D. Ahumada.

References

- Anca-Couce, A., Zobel, N., Jakobsen, H. A. (2013). Multi-scale modeling of fixed-bed thermo-chemical processes of biomass with the representative particle model: Application to pyrolysis. *Fuel* 103, 773-782. <https://doi.org/10.1016/j.fuel.2012.05.063>.
- Aramideh, S., Xiong, Q., Kong, S. C., Brown, R. C. (2015). Numerical simulation of biomass fast pyrolysis in an auger reactor. *Fuel* 156, 234-242. <https://doi.org/10.1016/j.fuel.2015.04.038>.
- Baggio, P., Baratieri, M., Fiori, L., Grigiante, M., Avi, D., Tosi, P. (2009). Experimental and modeling analysis of a batch gasification/pyrolysis reactor. *Energy Conversion and Management* 50(6), 1426-1435. <https://doi.org/10.1016/j.enconman.2009.03.004>.
- Baratieri, M., Baggio, P., Fiori, L., Grigiante, M. (2008). Biomass as an energy source: thermodynamic constraints on the performance of the conversion process. *Bioresour Technol* 99(15), 7063-7073. <https://doi.org/10.1016/j.biortech.2008.01.006>.
- Bhutto, A. W., Bazmi, A. A., Zahedi, G. (2011). Greener energy: Issues and challenges for Pakistan-Biomass energy prospective. *Renewable and Sustainable Energy Reviews* 15(6), 3207-3219. <https://doi.org/10.1016/j.rser.2011.04.015>.
- Bilgen, S. (2014). Structure and environmental impact of global energy consumption. *Renewable and Sustainable Energy Reviews* 38, 890-902. <https://doi.org/10.1016/j.rser.2014.07.004>.
- Bridgwater, A. V. (1994). Catalysis in thermal biomass conversion. *Applied Catalysis A: General* 116(1-2), 5-47. [https://doi.org/10.1016/0926-860X\(94\)80278-5](https://doi.org/10.1016/0926-860X(94)80278-5).
- Cabrera, A., Cox, L., Spokas, K., Hermosin, M. C., Cornejo, J., Koskinen, W. C. (2014). Influence of biochar amendments on the sorption-desorption of aminocyclopyrachlor,

- bentazone and pyraclostrobin pesticides to an agricultural soil. *Science of the Total Environment* 470, 438-443. <https://doi.org/10.1016/j.scitotenv.2013.09.080>.
- Di Blasi, C. (2000). Modelling the fast pyrolysis of cellulosic particles in fluid-bed reactors. *Chemical Engineering Science* 55(24), 5999-6013. [https://doi.org/10.1016/S0009-2509\(00\)00406-1](https://doi.org/10.1016/S0009-2509(00)00406-1).
- Gera, D., Mathur, M. P., Freeman, M. C., Robinson, A. (2002). Effect of large aspect ratio of biomass particles on carbon burnout in a utility boiler. *Energy & Fuels* 16(6), 1523-1532. <https://doi.org/10.1021/ef0200931>.
- Gidaspow, D. (1994). Multiphase flow and fluidization: continuum and kinetic theory descriptions. Academic press, ISBN: 9780122824708.
- Gorenssek, M. B., Shukre, R., Chen, C. C. (2019). Development of a thermophysical properties model for flowsheet simulation of biomass pyrolysis processes. *ACS Sustainable Chemistry and Engineering* 7(9), 9017-9027. <https://doi.org/10.1021/acssuschemeng.9b01278>.
- Gunn, D. J. (1978). Transfer of heat or mass to particles in fixed and fluidised beds. *International Journal of Heat and Mass Transfer* 21(4), 467-476. [https://doi.org/10.1016/0017-9310\(78\)90080-7](https://doi.org/10.1016/0017-9310(78)90080-7).
- Hertwich, E. G., Zhang, X. (2009). Concentrating-solar biomass gasification process for a 3rd generation biofuel. *Environmental Science & Technology* 43(11), 4207-4212. <https://doi.org/10.1021/es802853g>.
- Hornung, A., Dasappa, S. (2014). Thermochemical conversion of biomass. *Transformation of Biomass: Theory to Practice*. John Wiley & Sons Ltd.
- Janse, A. M. C., Westerhout, R. W. J., & Prins, W. (2000). Modelling of flash pyrolysis of a single wood particle. *Chemical Engineering and Processing: Process Intensification* 39(3), 239-252. [https://doi.org/10.1016/S0255-2701\(99\)00092-6](https://doi.org/10.1016/S0255-2701(99)00092-6).
- Kalgo, A. S. (2011). The development and optimisation of a fast pyrolysis process for bio-oil production. PhD Thesis. Aston University. Birmingham, UK.
- Kan, T., Strezov, V., Evans, T. J. (2016). Lignocellulosic biomass pyrolysis: A review of product properties and effects of pyrolysis parameters. *Renewable and Sustainable Energy Reviews* 57, 1126-1140. <https://doi.org/10.1016/j.rser.2015.12.185>.
- Lun, C. K. K., Savage, S. B., Jeffrey, D. J., Chepurniy, N. (1984). Kinetic theories for granular flow: inelastic particles in Couette flow and slightly inelastic particles in a general flowfield. *Journal of Fluid Mechanics* 140, 223-256. <https://doi.org/10.1017/S0022112084000586>.
- Mellin, P., Kantarelis, E., Yang, W. (2014). Computational fluid dynamics modeling of biomass fast pyrolysis in a fluidized bed reactor, using a comprehensive chemistry scheme. *Fuel* 117, 704-715. <https://doi.org/10.1016/j.fuel.2013.09.009>.
- Morales-Diaz, A., Vazquez-Sandoval, A. D., Carlos-Hernandez, S. (2015). analysis and control of a distributed parameter reactor for pyrolysis of wood. *Revista Mexicana de Ingeniería Química* 14(2), 543-552.
- Papadakis, K., Gu, S., Bridgwater, A. V., Gerhauser, H. (2009). Application of CFD to model fast pyrolysis of biomass. *Fuel Processing Technology* 90(4), 504-512. <https://doi.org/10.1016/j.fuproc.2009.01.010>.
- Palmay-Paredes, P. G., Morocho-Delgado, S., Puente-Guijarro, C., Donoso-Quimbata, C. (2021). Thermic pyrolysis of polypropylene waste as a source of fuel. *Revista Mexicana de Ingeniería Química* 20(2), 1019-1027. <https://doi.org/10.24275/rmiq/IA2321>.
- Ranganathan, P., Gu, S. (2016). Computational fluid dynamics modelling of biomass fast pyrolysis in fluidised bed reactors, focusing different kinetic schemes. *Bioresource Technology* 213, 333-341. <https://doi.org/10.1016/j.biortech.2016.02.042>.
- Ranz, W. E., Marshall, W. R. (1952). Evaporation from drops. *Chemical Engineering Progress* 48(3), 141-146.

- Ranzi, E., Cuoci, A., Faravelli, T., Frassoldati, A., Migliavacca, G., Pierucci, S., & Sommariva, S. (2008). Chemical kinetics of biomass pyrolysis. *Energy & Fuels* 22(6), 4292-4300. <https://doi.org/10.1021/ef800551t>.
- Raveendran, K., Ganesh, A., Khilar, K. C. (1995). Influence of mineral matter on biomass pyrolysis characteristics. *Fuel* 74(12), 1812-1822. [https://doi.org/10.1016/0016-2361\(95\)80013-8](https://doi.org/10.1016/0016-2361(95)80013-8).
- Rossi, A. (1984). Fuel Characteristics of Wood and Nonwood Biomass Fuels. In D. A. Tillman & E. C. Jahn (Eds.), *Progress in Biomass Conversion* (Vol. 5, pp. 69-99). Elsevier. <https://doi.org/10.1016/B978-0-12-535905-4.50008-4>.
- Schaeffer, D. G. (1987). Instability in the evolution equations describing incompressible granular flow. *Journal of Differential Equations* 66(1), 19-50. [https://doi.org/10.1016/0022-0396\(87\)90038-6](https://doi.org/10.1016/0022-0396(87)90038-6).
- Suleiman, Y., Ibrahim, H., Anyakora, N. V., Mohammed, F., Abubakar, A., Aderemi, B. O., Okonkwo, P. C. (2013). Design and fabrication of fluidized-bed reactor. *International Journal of Engineering and Computer Science* 2(5), 1595-1605.
- Syamlal, M., Rogers, W., O'Brien, T. J. (1993). MFIX documentation theory guide.
- Trendewicz, A., Braun R., Dutta A., Ziegler J. (2014). One dimensional steady-state circulating fluidized-bed reactor model for biomass fast pyrolysis, *Fuel* 133(1), 253-262. <https://doi.org/10.1016/j.fuel.2014.05.009>.
- Uchimiya, M., Klasson, K. T., Wartelle, L. H., Lima, I. M. (2011). Influence of soil properties on heavy metal sequestration by biochar amendment: 1. Copper sorption isotherms and the release of cations. *Chemosphere* 82(10), 1431-1437. <https://doi.org/10.1016/j.chemosphere.2010.11.050>.
- Wagenaar, B. M., Prins, W., Van Swaaij, W. P. M. (1994). Pyrolysis of biomass in the rotating cone reactor: modelling and experimental justification. *Chemical Engineering Science* 49(24), 5109-5126. [https://doi.org/10.1016/0009-2509\(94\)00392-0](https://doi.org/10.1016/0009-2509(94)00392-0).
- Weldekidan, H., Strezov, V., Town, G. (2018). Review of solar energy for biofuel extraction. *Renewable and Sustainable Energy Reviews* 88, 184-192. <https://doi.org/10.1016/j.rser.2018.02.027>.
- Xie, T., Reddy, K. R., Wang, C. W., Yargicoglu, E., Spokas, K. (2015). Characteristics and applications of biochar for environmental remediation: A review. *Critical Reviews in Environmental Science and Technology* 45(9), 939-969. <https://doi.org/10.1080/10643389.2014.924180>.
- Xiong, Q., Kong, S.-C., Passalacqua, A. (2013). Development of a generalized numerical framework for simulating biomass fast pyrolysis in fluidized-bed reactors. *Chemical Engineering Science* 99, 305-313. <https://doi.org/10.1016/j.ces.2013.06.017>.
- Xue, Q., Heindel, T. J., Fox, R. O. (2011). A CFD model for biomass fast pyrolysis in fluidized-bed reactors. *Chemical Engineering Science* 66(11), 2440-2452. <https://doi.org/10.1016/j.ces.2011.03.010>.
- Yang, Y. B., Sharifi, V. N., Swithenbank, J., Ma, L., Darvell, L. I., Jones, J. M., Pourkashanian, M., Williams, A. (2008). Combustion of a single particle of biomass. *Energy & Fuels* 22(1), 306-316. <https://doi.org/10.1021/ef700305r>.